Elastic stubbed metamaterial plate with torsional resonances

Wei Wang, Bernard Bonello, Bahram Djafari-Rouhani, Yan Pennec, Jinfeng Zhao

Elastic stubbed metamaterial plate with torsional resonances

Wei Wang[1], Bernard Bonello[1*], Bahram Djafari-Rouhani[2], Yan Pennec[2], and Jinfeng Zhao[3]

[1]Sorbonne Université, UPMC Université Paris 06 (INSP–UMR CNRS 7588),

4, place Jussieu 75005 Paris, France

[2]Institut d'Electronique, de Micro-électronique et de Nanotechnologie (IEMN–UMR CNRS 8520),

Université de Lille Sciences et Technologies, Cité Scientifique, 59652 Villeneuve d'Ascq Cedex, France

[3]School of Aerospace Engineering and Applied Mechanics, Tongji University,

100 Zhangwu Road, 200092 Shanghai, China

*corresponding author: bernard.bonello@insp.jussieu.fr

Abstract:

We report on a new mechanism involving the torsional resonance of stubs to achieve the negative effective shear modulus of an elastic metamaterial plate. Combined with a mechanism to create a negative mass density, we develop a general method to set up and enlarge a shear-horizontal-polarized double-negative branch in the elastic metamaterial plate with stubs on both sides. We explore the capabilities of this structure for polarization filtering, mode conversion and abnormal refraction. It is shown that, this metamaterial plate behaves divergently against the polarization of incident waves propagating along ΓX direction in a square lattice crystal: it behaves as a double-negative system for zero-order shear horizontal (SH_0) wave but as a single-negative one for zero-order antisymmetric (A_0) or symmetric (S_0) Lamb waves. Mode conversion is achieved when the propagation deviates from ΓX direction. Moreover, we observe abnormal refracted patterns with both positive and negative refraction occurring at the interface between a prism-shaped supercell and the surrounding plate. Furthermore, we propose a chiral pillar to efficiently couple the torsional resonance with an incident A_0 Lamb wave.

1. INTRODUCTION

The advent of locally resonant metamaterials almost two decades ago [1], and the great deal of research that ensue, have significantly contributed to the possibilities we have now for controlling both the propagation and the dispersion of the acoustic/elastic waves in the subwavelength scale [2–6]. Owing to the resonant designs, the effective elastic properties, *i.e.* mass density, bulk or shear modulus, of these artificial structures may become negative in narrow frequency bands [7,8]. Generally, the negative effective mass density relates to a dipolar resonance, as it is the case for instance in core-shell locally resonant rubber-lead-epoxy composites [1,9] or thin membranes [10,11] whereas the negative effective bulk modulus relates to monopolar resonances and can be realized by Helmholtz resonators [12] or multi-mass locally resonant inclusions in elastic configurations [13]. With regard to negative effective shear modulus, it may be associated to quadrupolar-like resonances, as reported in a fluid-

solid composite structure [14] or in elastic metamaterials [13,15]. However, different mechanisms and resonances can be involved in the determination of negative properties in thin metamaterial plates [16] where a general theory of effective parameters still needs more investigation. In particular, alternative mechanisms, not explored so far, may lead to negative effective shear modulus as well, as we demonstrate in this work.

Elastic stubbed metamaterials, constructed by assembling cylindrical pillars on a thin homogenous plate [17-19], have proved their efficiency in tailoring the propagation of Lamb waves [20–25] or shear-horizontal waves [26,27]. This ensues from the normal modes of the pillars, namely the bending, the compressional and the torsional modes, which each can well couple with Lamb or shear horizontal waves propagating in the plate. In particular, it has been reported that combining together in a common frequency interval the bending and the compressional resonances allows to achieve negative effective mass density in a single-sided stubbed metamaterial [28,29]. However, less attention has been paid to the torsional modes to date. Intuitively, in analogy to the rotational resonance of a core mass in a discrete mass-spring system that leads to negative effective stiffness [30,31], the torsional resonance of the pillars in the stubbed structure can be expected to well couple with the shear horizontal deformation in the plate and possibly leads to negative effective shear modulus. Furthermore, one may expect that the doubly negative property might be achieved in a double-sided stubbed metamaterial constructed by assembling two specific single-sided substructures, each supporting different resonant modes, in analogy to bulk systems [32]. This is the approach we have chosen in this work, where the stubs erected on one face of a plate support torsional resonances and allow the effective shear modulus to become negative, whereas the stubs on the opposite face endow the structure with negative effective mass density owing to the combination of their bending and compressional resonances. We show that the band structure of this original design features a narrow SH-polarized double-negative band where the torsional vibration of the pillars couple with SH_0 wave in the plate. The width of this band can be significantly enlarged if through holes are periodically drilled into the plate. Secondly, we investigate the transmission through a square lattice array of pillars for the three fundamental plate waves (SH_0, S_0 and A_0 modes) in the frequency range of the double-negative branch. We found that the stubbed metamaterial is well suited to engineer a polarization filter for incident waves propagating along ΓX direction. When the wave vector deviates from ΓX direction, mode conversion in the transmitted field is analyzed. Further, we numerically study the refraction of incident SH_0 wave at the outlet interface between a prism-shaped structure and the surrounding plate. The abnormal refracted patterns are analyzed owing to the equifrequency contours (EFCs) and the occurrence of either negative or both negative and positive refractions is demonstrated. Finally, to overcome the difficulty in exciting the torsional vibration with incident A_0 Lamb mode, we introduce chiral pillars in one face of the structure. Their effectiveness to perform this function is investigated by computing the transmission coefficient of A_0 Lamb mode.

2. BAND STRUCTURE OF ELASTIC PILLARED METAMATERIALS

2.1. Torsional resonance and effective shear modulus

The design to investigate the torsional vibration of a pillar on a plate, and more generally the band structure when this base structure is organized in a square lattice, is illustrated in the inset of Fig. 1(a). The dimensions of this unit cell were chosen such that the resonances occur in the MHz range. The diameter and the height of the pillar (hereafter denoted as pillar A) are d_A = 110 μm and h_A = 130 μm; the period of the lattice and the thickness of the plate are fixed to 200 μm and 100 μm respectively. Both the plate and the pillars were made of steel that has the double advantage of being isotropic and allowing for relatively easy fabrication of a sample. The Young's modulus, Poisson's ratio, and mass density are E = 200 GPa, ν = 0.3 and ρ = 7850 kg.m^{-3} respectively. We will refer to this single-sided pillared metamaterial as SPMA in the following.

The band structure computed using a finite element method is displayed in Fig. 1(a). Clearly, no complete band gap arises in the frequency range from 0 to 7 MHz. Instead, flat branches corresponding to the eigenmodes of the pillars occur around 5.3 MHz. These eigenmodes can be precisely identified by computing the associated displacement field. The corresponding motions at points Γ and M of the first Brillouin zone (BZ), and labelled as C and D in Fig. 1(a), are displayed in the right panel in Fig. 1(a). Unambiguously, pillar A undergoes an alternative torsional motion around its central axis, while the displacement in the plate is almost zero. Since a SH_0 wave propagating in the plate involves only a shear deformation, it is expected that it can couple with this mode. This is confirmed by the transmission spectrum of an incident SH_0 wave propagating across nine unit cells along ΓM direction and infinite along the normal to this direction (see inset in Fig.1(b)). For this calculation any wave reflected from the boundaries was eliminated by using a perfectly matched layer at each end of the structure. The physical parameters were the default values for steel implemented in the commercial code we used to perform the finite elements calculations (COMSOL Multiphysics). The incident wave was launched from the surface of the plate, at a distance of 1000 μm away from the left edge of the array of resonators that was impinged at normal incidence. Such a scheme exactly imitates the experimental layouts based on the use of either a pulsed laser [33] or a piezoelectric patch attached to the plate in front of the phononic crystal [34] in order to excite Lamb waves, thereby facilitating the direct comparison of the numerical data with forthcoming experimental results. The transmission coefficient, defined as the ratio of the displacement component along ΓM of the transmitted wave to the one of the plate without pillars is shown as a black solid line in Fig. 1(b): there is no transmission of this mode in the range from 5.29 to 5.35 MHZ. Similar behavior has been observed for the transmission spectrum along ΓX direction. Generally, such a low frequency (subwavelength) band gap can be interpreted in terms of negative effective property of the structure. In the present case, the geometry suggests that the torsional motion can couple with the local shear deformation of the plate, allowing in turn the effective shear modulus μ_{eff} to become negative. To

verify this assumption, we have calculated μ_{eff} using the numerical method described in Refs. [15,35,36]. In the calculation, we have considered a simple shear strain field applied along two parallel lateral boundaries of the unit cell. This sets the local displacement field and excites the torsional vibration of pillar A. The variation of μ_{eff} against the excitation frequency is then deduced from the equivalence between the work done by the induced forces on the lateral boundaries of the unit cell and the strain energy. The relationship between them can be expressed as $\sum \mathbf{F} \cdot \mathbf{U} = \frac{1}{2} \mu_{eff} \gamma^2 V$, where the summation runs over the lateral boundaries of the unit cell which volume is V and γ represents the amplitude of the applied shear strain. The result displayed as a red solid line in Fig. 1(b) (right scale) confirms that μ_{eff} is negative from 5.29 to 5.36 MHz, in very good agreement with the frequency interval in between points D (5.29 MHz) and C (5.35 MHz).

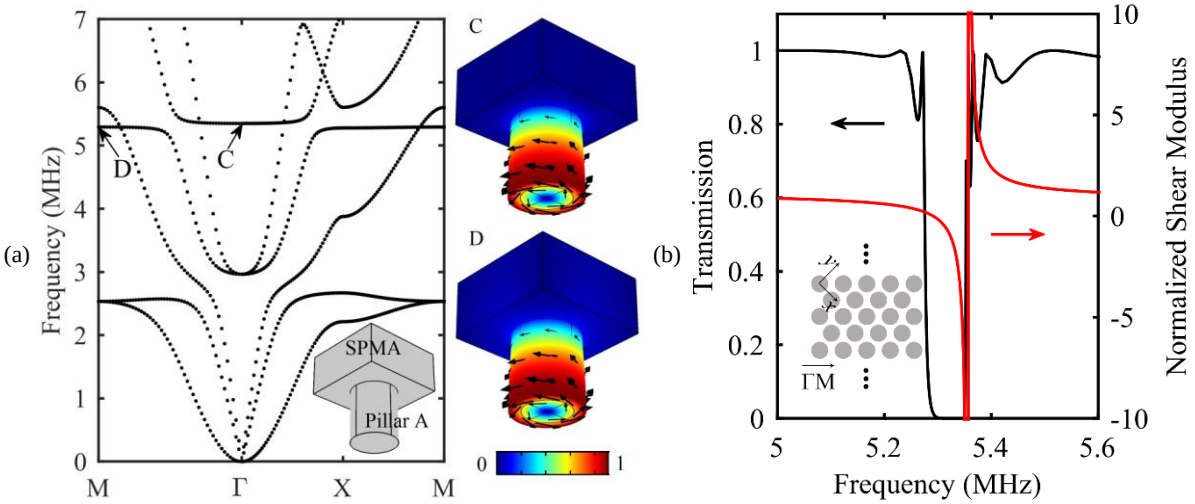

Figure 1: (a) Band structure of the single-sided stubbed metamaterial (SPMA) when arranged in a square lattice; inset: unit cell. The right panel shows the eigenmodes at point C and D. (b) left scale: Transmission spectrum of an incident SH_0 wave propagating through nine unit cells along ΓM direction (black solid line); right scale: normalized effective shear modulus of SPMA (red solid line). Inset: Schematic of the geometry used to calculate the transmission.

This naturally raises the question of whether it is possible to get the doubly negative property with such a structure. It has been demonstrated that double negativity can be achieved by combining two different substructures, each supporting different resonant modes [32]. Remembering that the combination of the compressional and the bending resonances of a pillar can lead to the negative effective mass density of the whole structure [29], it can be expected that a double-negative branch might be obtained by integrating a second pillar with suitable dimensions in the unit cell.

2.2. Bending and compressional resonances, and effective mass density – Double negativity

It has been shown in Ref. [24] that the first order compressional mode and the second order bending mode of a single pillar on a plate may occur in the same frequency interval, provided that the dimensions are carefully chosen. In that situation, the combination of these two resonant modes can

generate negative effective mass density as theoretically and numerically demonstrated in Ref. [29] contributing to a complete low frequency band gap. The structure depicted in the inset of Fig. 2 and denoted hereafter as SPMB, features a pillar with a diameter d_B = 80 μm and height h_B = 200 μm erected on a plate having the same size as SPMA. With these dimensions a band gap corresponding to a frequency range where the effective mass density gets negative, opens up in between 5.19 and 5.47 MHz in the BZ, as evidenced by the band structure shown in Fig. 2. This is further evidenced by the displacement fields shown in the right panel of Fig. 2, computed at points in the BZ labelled as E (bending) and F (compression). This interval comprises the frequency band where SPMA exhibits negative mass density and consequently the occurrence of double negativity may be expected from the merging of both structures.

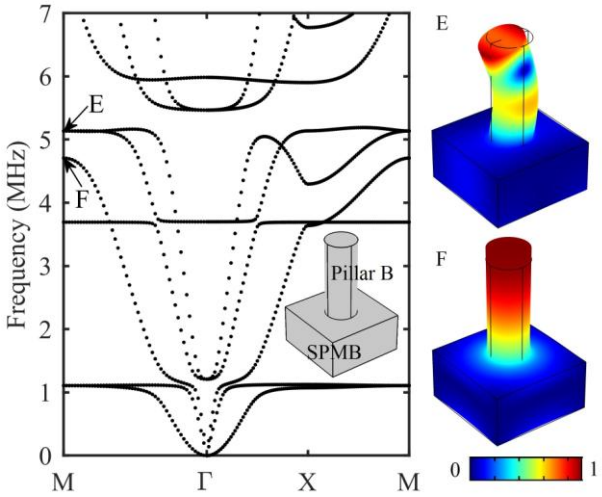

Figure 2: Band structure of the single-sided stubbed metamaterial (SPMB) when arranged in a square lattice; Inset: unit cell. The right panel shows the eigenmodes at points E and F.

To check the occurrence of a double negativity, we have computed the band structure of the asymmetric double-sided pillared metamaterial (DPM) in the inset of Fig. 3 that includes both pillar A and pillar B. The result is displayed in Fig. 3. As expected, an isolated branch, highlighted in red in this figure, appears in between 5.28 and 5.35 MHz. Note that this branch is not totally flat and rather features a negative-slope corresponding to a group velocity of about 40 ms^{-1} that can be relevant in some applications requiring a delay line. Additionally, we show the eigenmodes at some characteristic points, labelled from C' to F' in Fig. 3. At point M of the first BZ, both the bending (point E) and the compressional modes (point F) in Fig. 1(a) slightly shift to points E' and F' upon attachment of pillar A to the plate. For both these resonances, the displacement fields of DPM displayed in Fig. 3 show that the deformation of pillar A is very small at the compressional resonance and even null at the bending resonance. This suggests that pillar A acts as an inert mass attached to the plate that simply shifts the resonant frequencies of pillar B. Accordingly, the frequency interval of the negative effective mass density generated by resonances E' and F' of pillar B in DPM also shifts and appears now in between

5.21 and 5.48 MHz instead of 5.19 to 5.47 MHz in SPMB alone, but the overall mechanism leading to the negative effective mass density is the same for both structures.

With regard to the eigenfrequencies at points labelled as C and D in Fig. 1(a), they remain unchanged upon merging the two pillars into a single structure because there is no coupling between the torsional vibration of pillar A and the bending and the compressional vibrations of pillar B. For a sake of consistency in the notations, these points are labelled as C' and D' in Fig. 3. As mentioned before, the effective shear modulus turns negative in the frequency interval between these two points. Therefore, both the negative effective mass density and shear modulus are achieved in this narrow interval which perfectly explains the occurrence of the propagative branch with a negative-slope in Fig. 3.

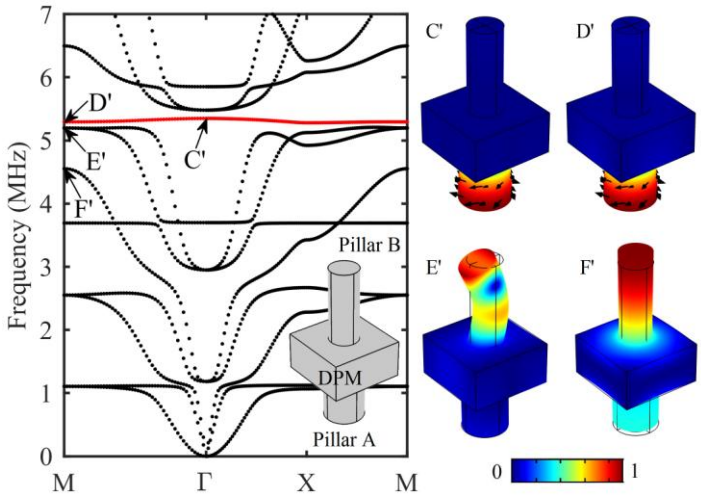

Figure 3: Band structure of the double-sided stubbed metamaterial (DPM) when arranged in a square lattice and the unit cell (see the inset). The right panel shows the eigenmodes at points from C' to F'.

However, it should not be assumed from the displacement fields at C' and D' that the negativity of shear modulus merely relates to the torsional eigenmode of pillar A. As a proof of this, Fig. 4(a) displays the eigenmode of the unit cell at the wave vector in the middle of ΓM. While pillar A vibrates on its torsional mode, the motion of pillar B clearly corresponds to the bending resonance. Moreover, the top view shown in the right panel reveals that the vibration lies in the plane perpendicular to the direction of propagation, which suggests that the doubly negative branch is SH polarized. This is further confirmed by the eigenmode computed at the wave vector in the middle of ΓX and shown in Fig. 4(b): here again, pillar B vibrates on its bending mode with a motion lying in the plane perpendicular to the direction of propagation, as better illustrated in the top view displayed in the right panel of Fig. 4(b), confirming that the branch is SH polarized. At this point of the BZ, the amplitude of the torsional motion of pillar A is relatively small but non-null from which it can be concluded that both the bending mode of pillar B and the torsional mode of pillar A contribute to the formation of the doubly negative branch.

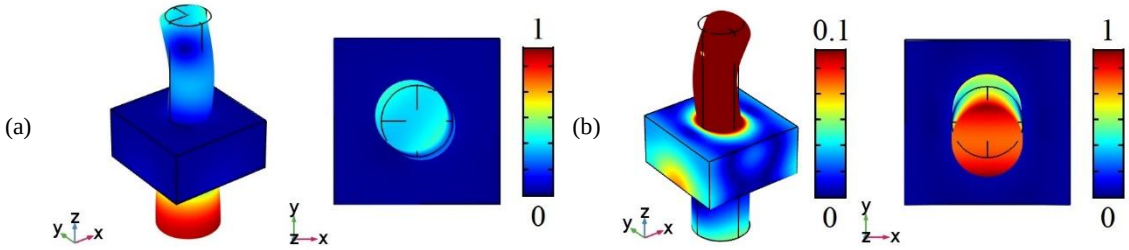

Figure 4: Eigenmodes of the unit cell for the wave vector in the middle of ΓM (a) and ΓX (b). The color scale is adapted to highlight the torsional motion. Their top views are shown in the corresponding right panels.

2.3. Enlargement of the doubly negative branch

In Sec. II-B, we have demonstrated the occurrence in DPM of the doubly negative property that ranges from 5.28 to 5.35 MHz. In some specific applications and devices where a high selectivity in frequency is a requirement, this narrow interval may be an advantage but there are other applications where a broad band is preferable instead. To establish that the stubbed metamaterials we have investigated in this work are able to meet such opposite requirements, we have improved the design of the structure by including holes drilled throughout the plate to enlarge the doubly negative branch. Actually, Bilal *et al.* [37] have established that the subwavelength band gaps can be increased by a factor of 4 in a perforated pillared plate. Such local resonance amplification phenomenon is sometimes called the trampoline effect. In this section, we examine the impact of these holes on the width of the doubly negative branch. Four through-holes with a diameter of 60 µm are drilled at the four corners of the unit cell of DPM. The band structure is displayed in Fig. 5(a) as red dotted lines. For comparison, the band structure of DPM without hole is also shown in Fig. 5(a) as black dotted lines. Both band structures share almost the same profile. In particular, the doubly negative branch along ΓX direction is not affected by the holes. Along ΓM direction, the eigenfrequency at point D' decreases to point D" because of the softening of the plate, logically leading to the increase by a factor of 2.3 of the width of the band where the effective shear modulus is negative that extends now from 5.19 to 5.35 MHz. Fig. 5(b) shows the band structure when the diameter of the holes is enlarged up to 100 µm. Both the eigenfrequencies of the bending mode and the compressional mode significantly shift downward. The frequency of the eigenmode at point D' is strongly impacted and moves down to point D'" and the doubly negative property occurs now in between 5.07 and 5.33 MHz allowing for a broader propagative band (the width is increased by a factor of 3.7). Note that this approach also applies to the chiral configuration described in Sec. IV.

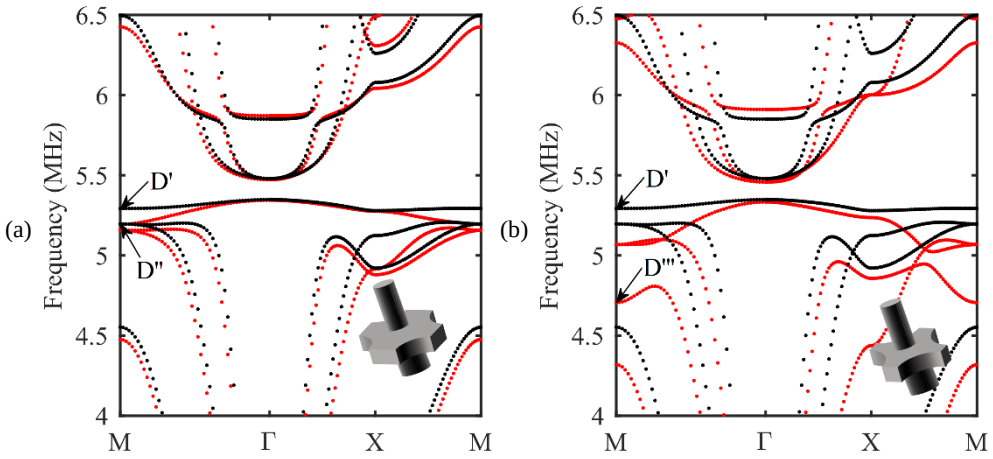

Figure 5: Band structures (red dotted lines) after introducing perforated holes with diameter 60 µm (a) and 100 µm (b) at the four corners of the unit cell of DPM. The band structure of DPM (without perforated holes) is shown as black dotted lines for reference.

3. FUNCTIONALITIES RELATED TO THE DOUBLE NEGATIVITY

3.1. Transmission dependence on the incident wave at the double negative branch

The isolated propagative branch being SH-polarized, it is quite natural to investigate the transmission of SH_0 wave through a structure of finite dimension along one direction of space and in turn, the coupling of this wave with both the torsional and the bending modes of the pillars. We thus have considered a metamaterial consisting of nine unit cells along *x*-axis and infinite along *y*-axis to investigate the propagation along ΓX direction [Fig. 6(a)]. The transmission coefficient, is displayed in Fig. 6(b) as a black solid line. This coefficient is almost equal to unity in the frequency interval where the doubly negative property occurs, which confirms that both the bending motion of pillar B and the torsional vibration of pillar A are efficiently excited. For comparison, Fig. 6(b) displays as red solid line the transmission coefficient of an incident A_0 Lamb wave normalized to the out-of-plane component of the incident wave. In the frequency interval where the double negativity occurs, the transmission coefficient is equal to zero. Symmetry considerations well explain this result. Actually, both the deformation caused by the elastic wave and the geometry of the structure are symmetric about the plane (*x*, *z*). This makes it impossible the coupling with the bending mode of pillar B in the plane perpendicular to the direction of propagation and thus the doubly negative branch turns to be a band gap. Similar conclusions can be drawn for an incident S_0 Lamb wave, even though its in-plane component is larger than its antisymmetric counterpart. To conclude this section, it should be noted that one can take advantage of the different behaviors along ΓX direction observed for incident SH_0 and A_0 or S_0 Lamb waves to conceive new polarization filter device [38] based on the geometry of the proposed DPM.

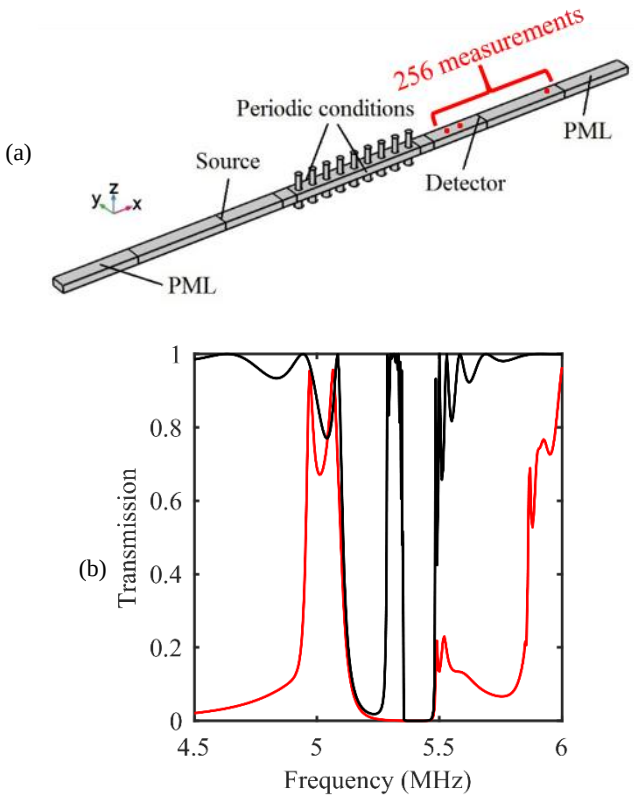

Figure 6: (a) Finite element model to investigate the transmission of incident SH_0 and A_0 Lamb waves along ΓX direction. (b) Transmission spectrum of an incident SH_0 wave (black solid line) and A_0 Lamb wave (red solid line) propagating across the supercell in (a).

3.2. Mode conversion

Jin *et al.* have established in Ref [24] that a pillar reemits Lamb waves when it is excited on either a bending or a compressional eigenmode. One must therefore question the nature of the transmitted waves in Fig. 6(a) and investigate possible mode conversions resulting from the interactions of the pillar at resonances with SH_0 wave propagating in the plate. The analysis is based on the fact that both S_0 and A_0 modes have an out-of-plane component, contrary to SH_0 mode that is in-plane polarized. The computation is performed for the propagation along different directions in the first BZ.

When the propagation is along ΓX direction (*i.e.* $k_y = 0$) at a frequency in the propagative branch (*i.e.* $\omega/2\pi$~5.33 MHz), the out-of-plane component u_z in the transmitted field, computed at the point called "detector" in Fig. 6(a), is null, within the computation accuracy, and only u_y has a measurable value. Let us note here that mode conversion cannot occur for propagation along this direction since, as shown above, the bending vibration of pillar B lies in the plane (y, z) in that case. Therefore, the wave vector of the reemitted wave is along y-axis; this is why the displacement field in the unstructured area downstream the pillars does not feature any out-of-plane component. In contrast an out-of-plane component u_z comes out in the transmitted field, when the incident wave vector slightly deviates from ΓX direction and has therefore a non-null component k_y. For instance, when $k_y = 0.05\pi/a$, the

component along z-axis in the transmitted field u_z, normalized to the amplitude U_y of the incident SH_0 wave, is different from zero and reads $u_z/U_y = 0.08$, which suggests the occurrence of A_0 and/or S_0 modes in the transmitted field. Accordingly, the normalized amplitudes of the in-plane components u_x and u_y are $u_x/U_y = 0.12$ and $u_y/U_y = 0.98$. These ratios go up to $u_z/U_y = 0.29$, $u_x/U_y = 0.41$ and $u_y/U_y = 0.75$ when $k_y = 0.2\pi/a$. An efficient way to identify the exact nature of the modes in the transmitted field is to compute their dispersion $\mathbf{k}(\omega)$ for frequencies in the double negative propagative branch. To this end, an incident SH_0 wave with $k_y = 0.2\pi/a$ at a frequency in the range where the double negativity occurs and with the amplitude U_y, is excited in front of the structure shown in Fig. 6(a). Both the components u_x and u_z of the displacement field in the homogeneous plate behind the pillars, are then computed at 256 different positions along the direction of propagation, separated by 50 µm from one another, as summarized in red in Fig. 6(a). The spatial Fourier transform of the data normalized to the amplitude of the incident SH_0 wave, $\mathcal{F}\left(u_{x,z}/U_y\right)$, allows to identify the elastic modes. The results for u_x and u_z at 5.33 MHz against the magnitude of the wave vector $\mathbf{k}$ are displayed in Figs. 7(a) and 7(b) respectively. The peak at $k = 0.01\mu m^{-1}$ in Fig. 7(a) evidently corresponds to SH_0 mode transmitted through the periodic structure. In addition, two other peaks at $k = 6.5\times10^{-3}$ and $k = 17.6\times10^{-3}\mu m^{-1}$ appear in the dispersion curves. These peaks correspond to S_0 and A_0 modes respectively, which clearly demonstrates the occurrence of mode conversion towards both A_0 and S_0 modes during the transmission of SH_0 mode through the structure when the wave vector deviates from ΓX direction. This is further confirmed by the out-of-plane component u_z against k displayed in Fig. 7(b): the curve features two sharp peaks at the wave vectors k corresponding to A_0 and S_0 modes which are both polarized in the sagittal plane.

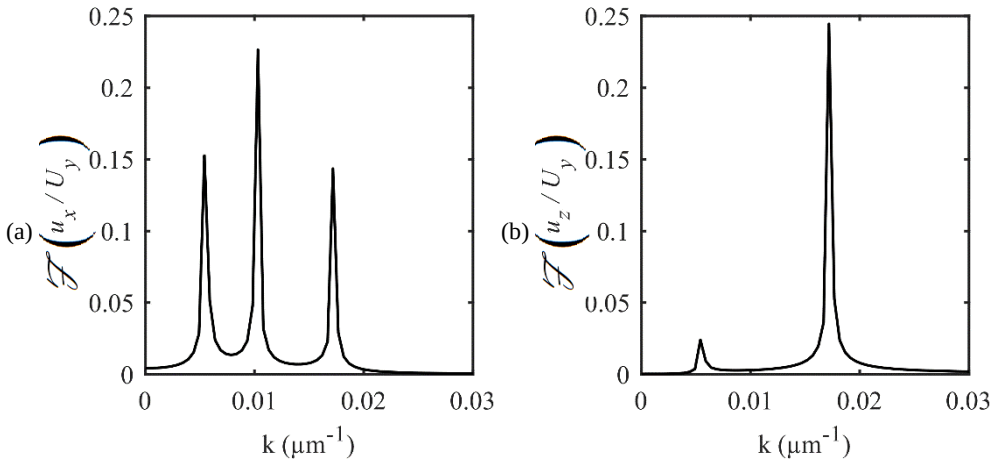

Figure 7: Magnitude of the Fourier spectrum of the displacement components, normalized to the incident amplitude, along *x*-axis (a) and *z*-axis (b) of the transmitted wave at 5.33 MHz.

3.3. Abnormal refraction of Lamb waves

The theoretical prediction and experimental observation of negative refraction of Lamb waves and shear-horizontal waves have been reported in elastic phononic crystals [33,39,40] and metamaterials [2,3,15]. In the former case, negative refraction relates to the periodicity and the resulting band folding, and therefore the wavelength of the refracted wave is of the same order of magnitude as the lattice constant. In contrast, in an elastic metamaterial, negative refraction is the direct consequence of simultaneously negative effective mass density and modulus (or stiffness) [2,3,15] and observing the phenomenon in the long-wavelength limit provides further evidence of the doubly negative property.

For this purpose, we have investigated the refraction of an incident SH_0 wave at the interface between a two-dimensional prism-shaped DPM and the surrounding plate. We shall discuss the occurrence in the transmitted waves of positively or negatively refracted SH_0, S_0 and A_0 modes. The structure depicted in Fig. 8(a) consists of 120 unit cells arranged in a 45° isosceles triangle in a circular steel plate. The plate is surrounded by a PML to eliminate any reflection from the boundaries. The two perpendicular boundaries of the prism are set parallel to the lattice directions ΓX and XM. A line source of width 1600 μm is placed 100 μm away from the inlet interface perpendicularly to ΓX direction and the wave impinged the prism at normal incidence. After propagation along *x*-axis in the prism, SH_0 wave is refracted but also reflected at the outlet interface and the latter propagates now along the negative direction of *y*-axis. This reflected SH_0 wave can couple with the bending vibration of pillar B in the plane (*x*, *z*), which in turn allows for reemission along the positive direction of *x*-axis of both A_0 and S_0 Lamb modes. Therefore, both these modes should be expected in the transmitted field, besides SH_0 mode. Two frequencies in close vicinity in the doubly negative branch were investigated, namely 5.31 and 5.33 MHz [Fig. 8(b)]. At these frequencies the wavelength of SH_0 mode is about 2.9 times the lattice constant, against 4.9 and 1.8 times the lattice constant for S_0 and A_0 modes respectively.

At 5.33 MHz, the out-of-plane component u_z in the transmitted field is displayed in Fig. 8(b). The occurrence of a negatively refracted wave at the outlet interface provides an evidence that both the effective mass density and shear modulus are simultaneously negative at this frequency. More surprisingly, a large part of incident wave is positively refracted, which cannot be explained without the help of mode conversion evidenced above. To show this, we have analyzed the propagation of waves in the reciprocal space [23,40] and computed the EFCs in DPM and in the surrounding medium. The approach consists of separately considering the symmetric S_0 and antisymmetric A_0 Lamb modes, which both feature an out-of-plane polarization, and are thus necessarily present in the transmitted fields shown in Fig. 8(b). Let us first consider A_0 mode. EFCs from 5.3 to 5.34 MHz in DPM, are displayed in Fig. 8(c) as grey solid lines (blue solid line at 5.33 MHz); the red circle is for EFC at 5.33 MHz in the plate and the cyan dashed line represents the normal to the outlet interface. Noticing that EFCs shrink as the frequency increases and using the conservation of the component of the wave

vector parallel to the interface, it is straightforward to draw the wave vector in the plate [red arrow labelled $\mathbf{k_A}$ in Fig. 8(c)], as well as the group velocities in DPM and in the plate which both are normal to EFCs (blue and red bold arrows labelled $\mathbf{V_g}$ and $\mathbf{V_{gA}}$ respectively). This simple scheme well accounts for the negative refracting angle $\theta_{(-)} = 17.2°$ measured at the outlet interface of DPM [see Fig. 8(b)] but not for the positive one. To explain the positive refraction one must consider **k** vector in DPM beyond the first BZ, as depicted in Fig. 8(d). Within this scheme of refraction, the relationship between **k** and $\mathbf{V_g}$ inside the doubly negative branch remains satisfied, namely $\mathbf{k} \cdot \mathbf{V_g} < 0$. Moreover, the conservation of the wave vector along the outlet interface leads to a transmitted wave refracted with the positive angle $\theta_{(+)} = 75.7°$.

Regarding the refraction at 5.31 MHz, the mechanism is exactly the same: A_0 Lamb mode features a wave vector forming an angle with the normal to the outlet interface either positive or negative, the only difference lying in the refractive angles (see Table. 1).

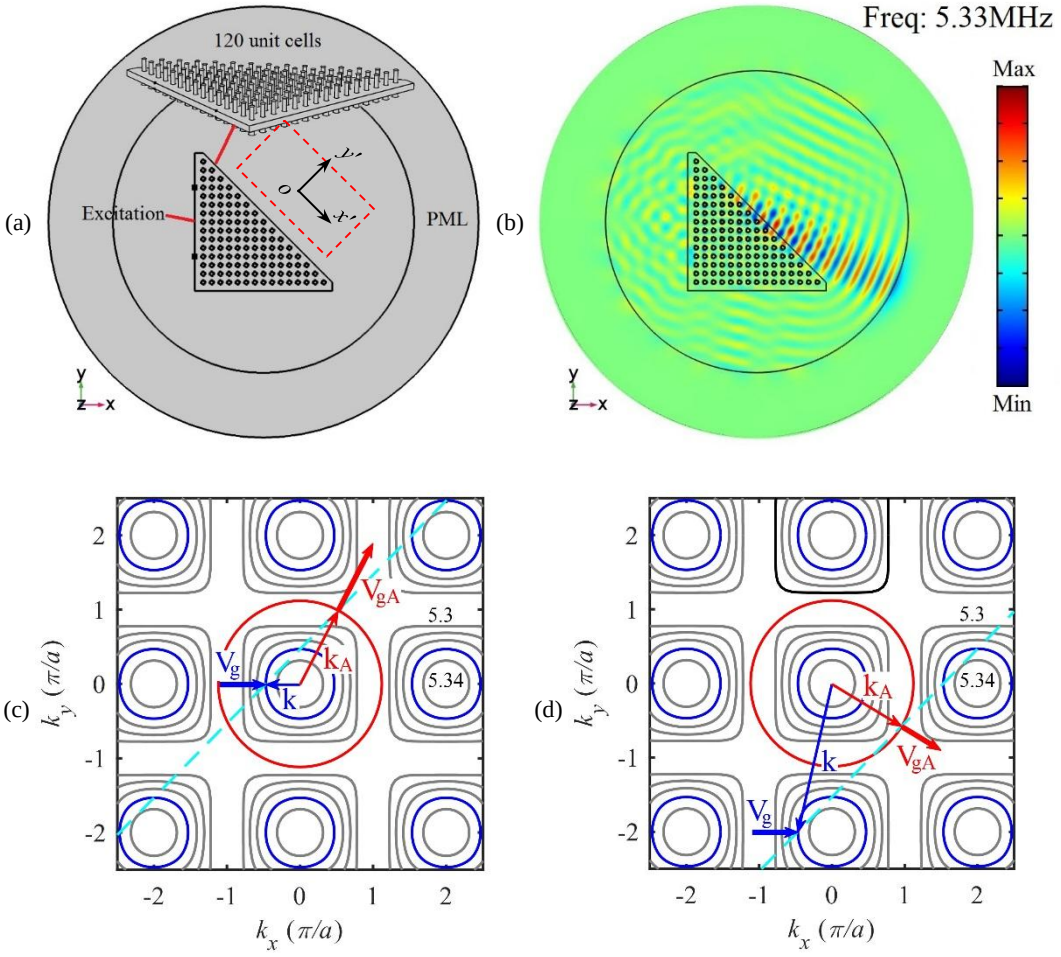

Figure 8: (a) Finite element model adopted to investigate the refraction at the outlet interface between a prism-like supercell and its surrounding plate. (b) Plot of the out-of-plane component on the top surface of the plate under the excitation of incident SH_0 mode at 5.33 MHz. EFCs analysis of the negative (c) and the positive (d) refraction at the outlet interface. The transmitted wave is assumed to be A_0 mode only.

Next, we assume that the transmitted wave only consists of S_0 mode and we analyze the refraction at 5.33 and 5.31 MHz following the same procedure as for A_0 mode. The results are displayed in Figs. 9(a) and 9(b) where the blue solid lines represent EFC in DPM and the magenta solid lines represent EFC in the surrounding plate at 5.33 and 5.31 MHz respectively. The group velocities and the wave vectors in DPM are denoted as $\mathbf{V_g}$ and $\mathbf{k}$ respectively. Both these quantities were calculated either at 5.33 MHz in Fig. 9(a) or at 5.31 MHz in Fig. 9(b). The symbols $\mathbf{V_{gS}}$ and $\mathbf{k_S}$ in Fig. 9(a) are for the group velocity and the wave vector at 5.33 MHz in the plate.

The refraction schemes for S_0 mode at 5.33 and 5.31 MHz are totally different from one another: whereas only the negative refraction at an angle of 54.9° occurs in the former case, no refracted beam, whether positive or negative, is observed in the latter case. This suggests the occurrence of abnormal refraction and that both symmetric and antisymmetric modes contribute to the out-of-plane component on the negative side of the normal to the outlet interface at 5.33 MHz, whereas only the antisymmetric mode gets refracted, both positively and negatively, if the frequency is lowered down to 5.31 MHz.

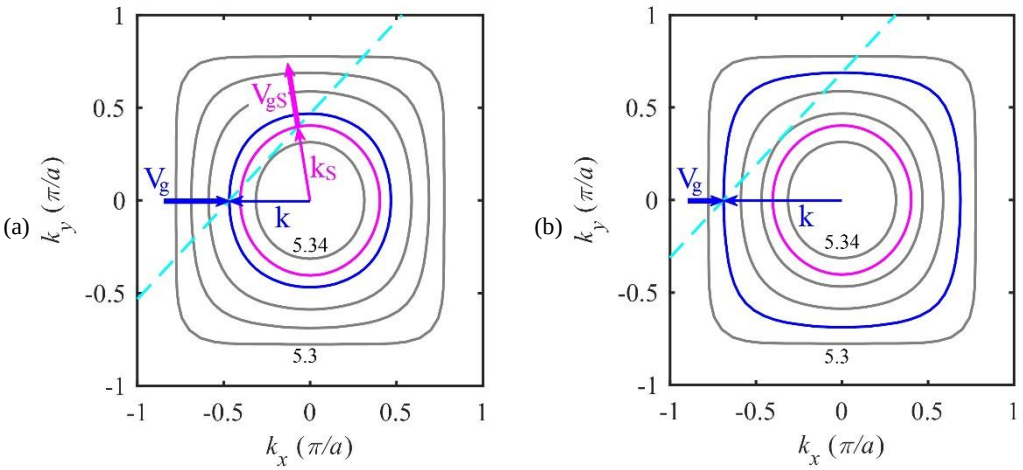

Figure 9: EFCs analysis of the refraction at the outlet interface at 5.33 (a) and 5.31 MHz (b). The transmitted wave is assumed to be S_0 mode only.

To further confirm this, we have computed the two-dimensional Fourier transform (2D FFT) of the out-of-plane component in the area surrounded by a red dashed line in Fig. 8(a). The computations were done in a local system of coordinates ($x'Oy'$) obtained by rotating the original system by 45° clockwise. The results at 5.33 and 5.31 MHz are displayed in Figs. 10(a) and 10(b) respectively. While both A_0 and S_0 modes are observed in Fig. 10(a), there is no contribution of S_0 mode in Fig. 10(b), which is consistent with the previous analysis that this mode can only be negatively refracted at 5.33 MHz whereas it is only reflected at 5.31 MHz. For comparison, the refractive angles calculated from EFCs analysis are displayed as red dashed lines for A_0 mode and magenta dashed line for S_0 mode. Both are in good agreement with 2D FFT results.

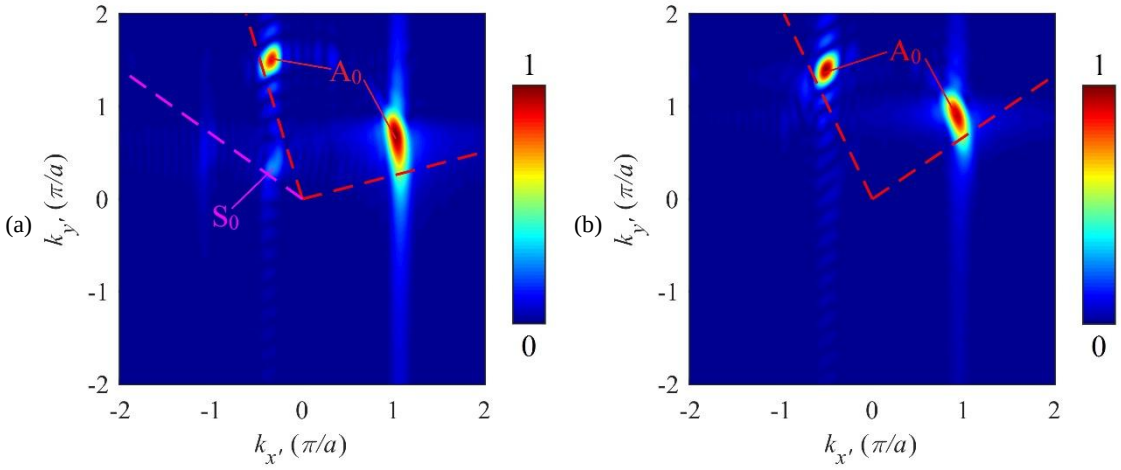

Figure 10: 2D FFT of the out-of-plane component in the red dashed area shown in Fig. 8(a) at 5.33 (a) and 5.31 MHz (b). The red and magenta dashed lines depict their refractive angles calculated from EFCs analysis.

With regard to the transmission of SH_0 mode, one must consider the in-plane components in the transmitted field. However, the analysis is rendered more difficult by the fact that both A_0 and S_0 modes also contribute to the in-plane motion downstream the outlet interface. To illustrate this, we show the in-plane components u_x and u_y on the top surface of the structure at 5.33 MHz in the left and right panels of Fig. 11(a) respectively: as previously, refraction on both sides of the normal to the outlet interface can be observed; however, as a result of the displacement fields associated to A_0 and S_0 modes whose polarization are close to *y*-axis [see Figs. 8(c) and 9(a)], the wave front of the negatively refracted beam in the right panel appears unstructured. The EFC analysis of SH_0 mode at 5.33 MHz (not shown here) clearly shows that this mode is negatively refracted at an angle of 29°, displayed as a green dashed line in Fig. 11(b).

The perpendicular polarization of the negatively refracted beam overlaps with both A_0 (17.2°) and S_0 modes (54.9°) to produce the complex pattern in the right panel of Fig. 11(a). Instead, the in-plane component u_x mainly contains SH_0 mode leading to the plane wave front in the negatively refracted beam. This is further confirmed by 2D FFT of the in-plane component u_x at 5.33 MHz, recorded in the rectangle area drawn in Fig. 8(a) and displayed in the left panel of Fig. 11(b). The refractive angle derived from 2D FFT is in good agreement with the result of EFCs analysis. The right panel of Fig. 11(b) shows 2D FFT of the in-plane component u_y. It can be seen that the positive refraction (*i.e.* $k_{x'}$ and $k_{y'}$ both positive) only includes A_0 mode whereas the negative refraction combines A_0, S_0, and SH_0 modes. 2D FFT performed at 5.31 MHz (not shown here) confirms that S_0 mode does not appear in the negative refraction part of the in-plane component map. Table. 1 summarizes all the refractive angles of A_0, S_0 and SH_0 modes.

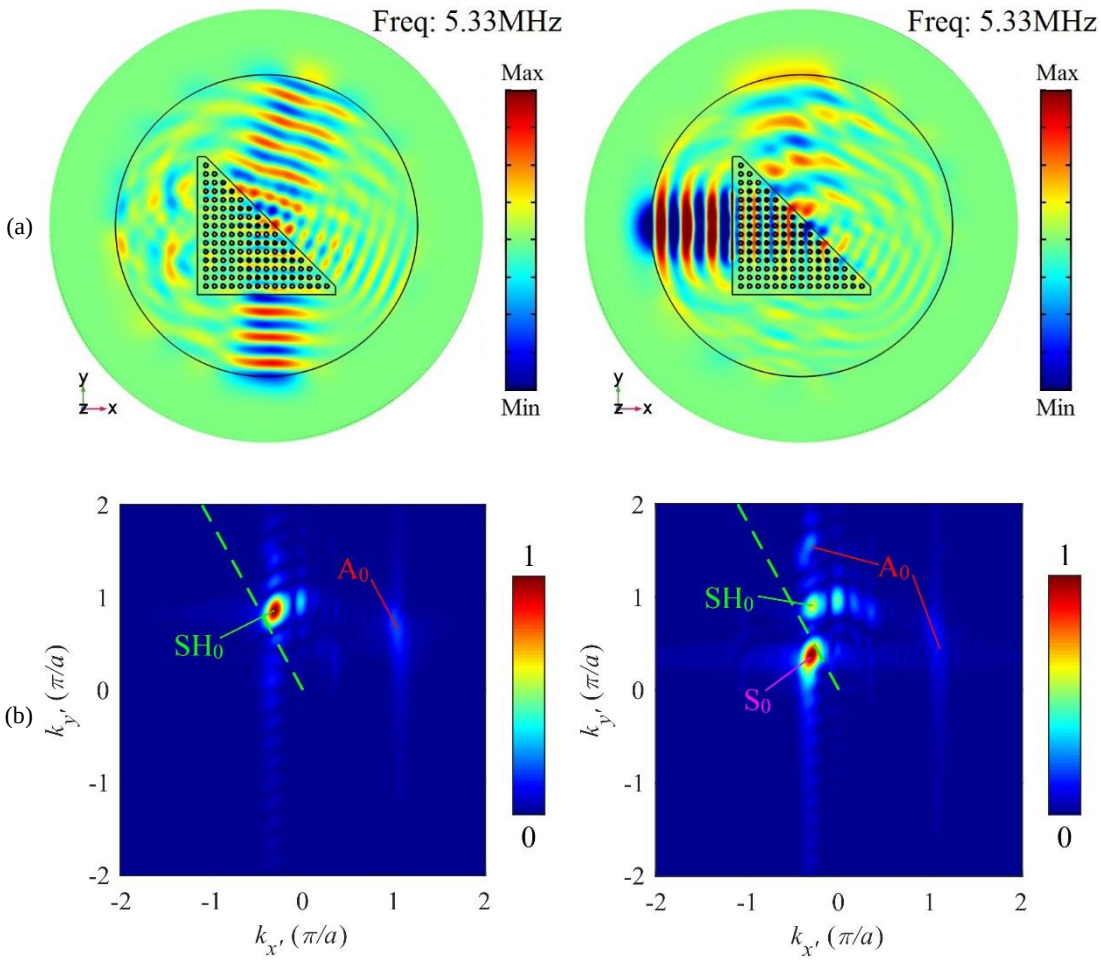

Figure 11: (a) Plots of the in-plane components u_x (left panel) and u_y (right panel) on the top surface of the plate under excitation by incident SH_0 mode at 5.33 MHz. (b) 2D FFT of the in-plane components u_x (left panel) and u_y (right panel) in the red dashed area shown in Fig. 8(a) at 5.33 MHz. The green dashed line depicts its refractive angle calculated from EFCs analysis.

Table 1. Summary of refractive angles when the transmission wave is assumed to be A_0, S_0 and SH_0 waves respectively at 5.31 and 5.33 MHz. Signs (+) and (–) refer to positive and negative refractions respectively.

Frequency (MHz)	A_0 (–)	A_0 (+)	S_0 (–)	S_0 (+)	SH_0 (–)	SH_0 (+)
5.31	25.9°	56.2°	/	/	45.9°	/
5.33	17.2°	75.7°	54.9°	/	29°	/

4. STUBBED METAMATERIAL WITH CHIRALITY

The preceding analysis in Sec. III-A unambiguously demonstrates that along ΓX direction the doubly negative property can be obtained with SH_0 wave whereas most of the applications proposed so far rely on the utilization of the dispersive A_0 or S_0 mode. This raises the issue of how to efficiently and simultaneously excite both the bending resonance of pillar B on one side and the torsional resonance of pillar A on the other side with A_0 or S_0 mode. The main difficulty comes from the excitation of the

torsional motion of pillar A. Once the torsional vibration of pillar A is excited, then the local shear deformation in the plate can easily excite the bending vibration of pillar B in the perpendicular plane.

An achievable solution to address this problem is to introduce chirality [41,42] to the pillar in order to break the symmetry of the unit cell. As a consequence, it is expected that the propagation of the waves in the plate results in an asymmetric deformation in the surrounding area of the pillar; that should easily lead to the torsional vibration especially when the frequency of the wave is close to the one of the torsional eigenmode. Although the chirality can be introduced in many ways, we propose here a chiral structure that exhibits a high coupling efficiency to the A_0 Lamb mode. Both the cross section and the side view of a pillar fulfilling this requirement are shown in Fig. 12(a). Eight flanks equally spaced in azimuth with a length l = 60μm and a width w = 10μm are inserted along a solid cylinder with diameter d = 100μm and height h = 105μm. A twist angle θ = 45° in anti-clockwise direction is further applied to each flanks, as shown in the bottom panel of Fig. 12(a). The band structure of this chiral double-sided stubbed metamaterial (CDPM) is displayed as red dotted lines in Fig. 12(b) together with the band structure of DPM which is displayed for comparison as black dotted lines. The band structure of CDPM has a profile similar to the one of DPM. The doubly negative branch goes from 5.37 to 5.41 MHz which is slightly different from DPM where the doubly negative branch goes from 5.28 to 5.35 MHz. The eigenmodes at points labelled as L, N, and P in Fig. 12(b) that correspond respectively to the bending and the compressional resonances of pillar B and to the torsional resonance of pillar A, are displayed in Fig. 12(d). Comparing these displacement fields to their counterparts in DPM [see the displacement fields at points E', F', C' in the right panel in Fig. 3] shows that the eigenmodes of the structure in the frequency domain of interest are conserved when introducing chirality in pillar A.

To further point out the efficiency of the chirality to excite the torsional vibration, we show as the red solid line in Fig. 12(c) the transmission spectrum of an incident A_0 mode propagating along ΓX through the supercell shown in Fig. 6(a) with chiral pillars on the bottom face of the plate. A transmission coefficient of about 0.25 is obtained in the frequency range where the doubly negative property occurs thanks to the combination of the bending vibration of pillar B and the torsional vibration of pillar A. This result must be compared with the transmission spectrum of A_0 mode which is null inside the doubly negative branch in the absence of chirality [see the red solid line in Fig. 6(b)] since the torsional resonance is not excited in that case.

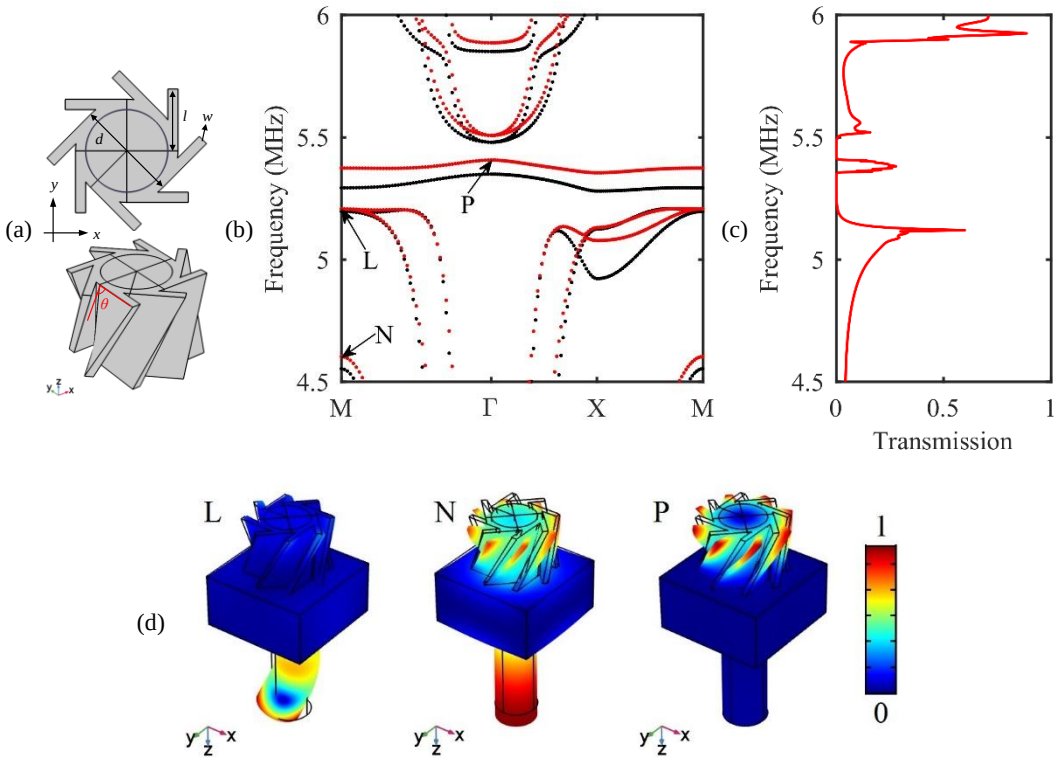

Figure 12: (a) Representative profile of the chiral pillar A. (b) Band structure of CDPM (red dotted lines) and DPM (black dotted lines). (c) Transmission spectrum of an incident A_0 mode propagating across the supercell shown in Fig. 6(a) with the chiral pillar A instead. (d) Eigenmodes of the unit cell corresponding to the points indicated in (b).

5. CONCLUSION

In this work, we have demonstrated a new resonance process, different from the quadrupolar-like one reported in Refs. [13–15], to achieve negative effective shear modulus. This new mechanism involves the torsional resonance of a pillar in the unit cell of an elastic stubbed metamaterial plate. In addition, we have presented a general method to obtain a SH polarized double-negative branch in the double-sided stubbed metamaterial plate showing great potential for polarization filtering, mode conversion and abnormal refraction. For that purpose, we first have designed a single-sided stubbed metamaterial whose torsional resonance (leading to negative effective shear modulus) is tuned to meet the requirement of the operating frequency. Then, we have introduced a second single-sided structure with carefully chosen parameters to ensure both the bending and the compressional resonances (contributing to negative effective mass density) occurring at the same frequency. Finally, by gathering two pillars in a single unit cell (attached on each side of the plate), the shear-horizontal double-negative branch can be achieved in the merged configuration. Besides, we show that the width of the doubly negative branch can be enlarged by a factor of 3.7 by simply employing perforated holes into the plate. Considering the transmission through a structure that is finite along *x*-axis and infinite along *y*-axis, SH_0 wave has proven to be the most suitable candidate. The proposed double-sided stubbed metamaterial shows polarization dependence for the propagation along ΓX direction. At the

doubly negative branch, incident SH_0 wave propagates without any measurable attenuation whereas incident A_0 or S_0 Lamb wave is totally reflected. Moreover, mode conversion is observed and studied by computing the displacement components of the transmitted wave when the wave vector deviates from ΓX direction. To highlight the occurrence of the doubly negative property, the refraction at the outlet interface between a prism-shaped structure and its surrounding plate is studied. Interestingly, both positive and negative refractions are observed. The physical explanation of this behavior is analyzed in details with the help of the EFCs. We show that the out-of-plane component in the positive refraction domain only involves A_0 mode. As for the negative refraction, at 5.33 MHz it involves both A_0 and S_0 modes, whereas at 5.31 MHz only A_0 mode is refracted. Finally, to overcome the difficulty of exciting the pillar into the torsional vibration with A_0 or S_0 mode, we have introduced the chirality into the unit cell, causing an asymmetric deformation in the surrounding area of the pillar. The efficiency of this method is further demonstrated by computing the transmission spectrum of an incident A_0 Lamb wave.

Acknowledgements

Wei Wang acknowledges the research scholarship No. 201608310130 provided by the China Scholarship Council.

References

[1] Z. Liu, X. Zhang, Y. Mao, Y.Y. Zhu, Z. Yang, C.T. Chan, P. Sheng, Locally resonant sonic materials, Science 289 (2000) 1734–1736.

[2] X.N. Liu, G.K. Hu, G.L. Huang, C.T. Sun, An elastic metamaterial with simultaneously negative mass density and bulk modulus, Appl. Phys. Lett. 98 (2011) 251907.

[3] R. Zhu, X.N. Liu, G.K. Hu, C.T. Sun, G.L. Huang, Negative refraction of elastic waves at the deep-subwavelength scale in a single-phase metamaterial, Nat. Commun. 5 (2014) 5510.

[4] J.B. Pendry, Negative refraction makes a perfect lens, Phys. Rev. Lett. 85 (2000) 3966–3969.

[5] S.A. Cummer, D. Schurig, One path to acoustic cloaking, New J. Phys. 9 (2007) 45.

[6] Y. Lai, H. Chen, Z.Q. Zhang, C.T. Chan, Complementary media invisibility cloak that cloaks objects at a distance outside the cloaking shell, Phys. Rev. Lett. 102 (2009) 093901.

[7] Y. Wu, Y. Lai, Z. Zhang, Effective medium theory for elastic metamaterials in two dimensions, Phys. Rev. B. 76 (2007) 205313.

[8] X. Zhou, G. Hu, Analytic model of elastic metamaterials with local resonances, Phys. Rev. B - Condens. Matter Mater. Phys. 79 (2009) 195109.

[9] Z. Liu, C.T. Chan, P. Sheng, Analytic model of phononic crystals with local resonances, Phys. Rev. B - Condens. Matter Mater. Phys. 71 (2005) 014103.

[10] Z. Yang, J. Mei, M. Yang, N.H. Chan, P. Sheng, Membrane-type acoustic metamaterial with negative dynamic mass, Phys. Rev. Lett. 101 (2008) 204301.

[11] M. Yang, G. Ma, Z. Yang, P. Sheng, Coupled membranes with doubly negative mass density and bulk modulus, Phys. Rev. Lett. 110 (2013) 134301.

[12] N. Fang, D. Xi, J. Xu, M. Ambati, W. Srituravanich, C. Sun, X. Zhang, Ultrasonic metamaterials with negative modulus, Nat. Mater. 5 (2006) 452.

[13] Y. Lai, Y. Wu, P. Sheng, Z.-Q. Zhang, Hybrid elastic solids, Nat. Mater. 10 (2011) 620.

[14] Y. Wu, Y. Lai, Z.Q. Zhang, Elastic metamaterials with simultaneously negative effective shear modulus and mass density, Phys. Rev. Lett. 107 (2011) 105506.

[15] H.-W. Dong, S.-D. Zhao, Y.-S. Wang, C. Zhang, Topology optimization of anisotropic broadband double-negative elastic metamaterials, J. Mech. Phys. Solids. 105 (2017) 54–80.

[16] D. Torrent, Y. Pennec, B. Djafari-Rouhani, Effective medium theory for elastic metamaterials in thin elastic plates, Phys. Rev. B - Condens. Matter Mater. Phys. 90 (2014) 104110.

[17] Y. Pennec, B. Djafari-Rouhani, H. Larabi, J.O. Vasseur, A.C. Hladky-Hennion, Low-frequency gaps in a phononic crystal constituted of cylindrical dots deposited on a thin homogeneous plate, Phys. Rev. B - Condens. Matter Mater. Phys. 78 (2008) 104105.

[18] T.T. Wu, Z.G. Huang, T.C. Tsai, T.C. Wu, Evidence of complete band gap and resonances in a plate with periodic stubbed surface, Appl. Phys. Lett. 93 (2008) 111902.

[19] T.-T. Wang, Y.-F. Wang, Y.-S. Wang, and V. Laude, Tunable fluid-filled phononic metastrip, Appl. Phys. Lett. 111 (2017) 041906.

[20] M. Oudich, M. Senesi, M.B. Assouar, M. Ruzenne, J.H. Sun, B. Vincent, Z. Hou, T.T. Wu, Experimental evidence of locally resonant sonic band gap in two-dimensional phononic stubbed plates, Phys. Rev. B - Condens. Matter Mater. Phys. 84 (2011) 165136.

[21] M.B. Assouar, J.H. Sun, F.S. Lin, J.C. Hsu, Hybrid phononic crystal plates for lowering and widening acoustic band gaps, Ultrasonics. 54 (2014) 2159–2164.

[22] F. Shu, Y. Liu, J. Wu, Y. Wu, Band gap in tubular pillar phononic crystal plate, Ultrasonics. 71 (2016) 172–176.

[23] J. Zhao, B. Bonello, O. Boyko, Focusing of the lowest-order antisymmetric Lamb mode behind a gradient-index acoustic metalens with local resonators, Phys. Rev. B. 93 (2016) 174306.

[24] Y. Jin, B. Bonello, R.P. Moiseyenko, Y. Pennec, O. Boyko, B. Djafari-Rouhani, Pillar-type acoustic metasurface, Phys. Rev. B. 96 (2017) 104311.

[25] Y. Li, L. Zhu, T. Chen, Plate-type elastic metamaterials for low-frequency broadband elastic wave attenuation, Ultrasonics. 73 (2017) 34–42.

[26] M.K. Lee, P.S. Ma, I.K. Lee, H.W. Kim, Y.Y. Kim, Negative refraction experiments with guided shear-horizontal waves in thin phononic crystal plates, Appl. Phys. Lett. 98 (2011) 011909.

[27] P. Li, L. Cheng, Shear horizontal wave propagation in a periodic stubbed plate and its application in rainbow trapping, Ultrasonics. 84 (2018) 244–253.

[28] M. Oudich, B. Djafari-Rouhani, Y. Pennec, M.B. Assouar, B. Bonello, Negative effective mass density of acoustic metamaterial plate decorated with low frequency resonant pillars, J. Appl. Phys. 116 (2014) 184504.

[29] W. Wang, B. Bonello, B. Djafari-Rouhani, Y. Pennec, J. Zhao, Double-Negative Pillared Elastic Metamaterial, Phys. Rev. Appl. 10 (2018) 064011.

[30] X. Wang, Dynamic behaviour of a metamaterial system with negative mass and modulus, Int. J. Solids Struct. 51 (2014) 1534–1541.

[31] Z. Li, X. Wang, On the dynamic behaviour of a two-dimensional elastic metamaterial system, Int. J. Solids Struct. 78 (2016) 174–181.

[32] Y. Ding, Z. Liu, C. Qiu, J. Shi, Metamaterial with simultaneously negative bulk modulus and mass density, Phys. Rev. Lett. 99 (2007) 093904.

[33] J. Pierre, O. Boyko, L. Belliard, J.O. Vasseur, B. Bonello, Negative refraction of zero order flexural Lamb waves through a two-dimensional phononic crystal, Appl. Phys. Lett. 97 (2010) 121919.

[34] Y.-F. Wang, T.-T. Wang, J.-P. Liu, Y.- S. Wang, V. Laude, Guiding and splitting Lamb waves in coupled-resonator elastic waveguides, Composite Structures 206, (2018) 588–593.

[35] X.N. Liu, G.K. Hu, C.T. Sun, G.L. Huang, Wave propagation characterization and design of two-dimensional elastic chiral metacomposite, J. Sound Vib. 330 (2011) 2536–2553.

[36] Y.-F. Wang, Y.-S. Wang, C. Zhang, Two-dimensional locally resonant elastic metamaterials with chiral comb-like interlayers: Bandgap and simultaneously double negative properties, J. Acoust. Soc. Am. 139 (2016) 3311.

[37] O.R. Bilal, M.I. Hussein, Trampoline metamaterial: Local resonance enhancement by springboards, Appl. Phys. Lett. 103 (2013) 111901.

[38] M. Miniaci, R.K. Pal, R. Manna, M. Ruzzene, Valley based splitting of topologically protected helical waves in elastic plates, Phys. Rev. B. 100 (2019) 024304.

[39] A. Sukhovich, L. Jing, J.H. Page, Negative refraction and focusing of ultrasound in two-dimensional phononic crystals, Phys. Rev. B - Condens. Matter Mater. Phys. 77 (2008) 014301.

[40] J. Bucay, E. Roussel, J.O. Vasseur, P.A. Deymier, A.C. Hladky-Hennion, Y. Pennec, K. Muralidharan, B. Djafari-Rouhani, B. Dubus, Positive, negative, zero refraction, and beam splitting in a solid/air phononic crystal: Theoretical and experimental study, Phys. Rev. B - Condens. Matter Mater. Phys. 79 (2009) 214305.

[41] D. Bigoni, S. Guenneau, A.B. Movchan, M. Brun, Elastic metamaterials with inertial locally resonant structures: Application to lensing and localization, Phys. Rev. B - Condens. Matter Mater. Phys. 87 (2013) 174303.

[42] A. Spadoni, M. Ruzzene, S. Gonella, F. Scarpa, Phononic properties of hexagonal chiral lattices, Wave Motion. 46 (2009) 435–450.